Sensitivity of Antarctic Bottom Water to Changes in Surface Buoyancy Fluxes

KATE SNOW AND ANDREW MCC. HOGG

Research School of Earth Sciences, and ARC Centre of Excellence for Climate System Science, Australian National University, Canberra, Australian Capital Territory, Australia

BERNADETTE M. SLOYAN

Ocean and Atmosphere Flagship, CSIRO, Hobart, Tasmania, Australia

STEPHANIE M. DOWNES

Research School of Earth Sciences, and ARC Centre of Excellence for Climate System Science, Australian National University, Canberra, Australian Capital Territory, and Antarctic Climate and Ecosystems Cooperative Research Centre, University of Tasmania, Hobart, Tasmania, Australia

(Manuscript received 5 July 2015, in final form 6 October 2015)

ABSTRACT

The influence of freshwater and heat flux changes on Antarctic Bottom Water (AABW) properties are investigated within a realistic bathymetry coupled ocean–ice sector model of the Atlantic Ocean. The model simulations are conducted at eddy-permitting resolution where dense shelf water production dominates over open ocean convection in forming AABW. Freshwater and heat flux perturbations are applied independently and have contradictory surface responses, with increased upper-ocean temperature and reduced ice formation under heating and the opposite under increased freshwater fluxes. AABW transport into the abyssal ocean reduces under both flux changes, with the reduction in transport being proportional to the net buoyancy flux anomaly south of 60°S.

Through inclusion of shelf-sourced AABW, a process absent from most current generation climate models, cooling and freshening of dense source water is facilitated via reduced on-shelf/off-shelf exchange flow. Such cooling is propagated to the abyssal ocean, while compensating warming in the deep ocean under heating introduces a decadal-scale variability of the abyssal water masses. This study emphasizes the fundamental role buoyancy plays in controlling AABW, as well as the importance of the inclusion of shelf-sourced AABW within climate models in order to attain the complete spectrum of possible climate change responses.

1. Introduction

Antarctic Bottom Water (AABW) is one of the densest and most voluminous water masses of the global ocean. It forms the lower limb of the meridional overturning circulation (MOC) and plays an important role in transporting carbon, heat, and freshwater sequestered from the atmosphere to the deep ocean (Johnson 2008; Kuhlbrodt et al. 2007; Ríos et al. 2012; Purkey and Johnson 2013). AABW source water is formed initially through surface buoyancy losses via cooling and brine rejection during winter sea ice formation where a reservoir of cold dense water may be established on the Antarctic continental shelf. The shelf water interacts and mixes with the warm, salty Circumpolar Deep Water (CDW) that intrudes onto the shelf, as well as with relatively cold meltwater from the base of marine ice shelves (Jacobs 2004). When the shelf water is denser than the open ocean and conditions favor overflow, the dense shelf water can spill over the continental shelf, further entraining CDW (Jacobs 2004), until reaching the abyssal ocean and flowing northward as AABW.

The process forming dense shelf water, a precursor to AABW, is absent from most current-generation climate models [e.g., those from phase 5 of the Coupled Model Intercomparison Project (CMIP5); Heuzé et al. 2015]. Most models rely on open ocean convection resulting from winter surface buoyancy losses within the Ross and

Corresponding author address: Kate Snow, Research School of Earth Sciences, Australian National University, Mills Rd., Acton ACT 2601, Australia.
E-mail: kate.snow@anu.edu.au

DOI: 10.1175/JCLI-D-15-0467.1

Weddell Seas to provide a source of dense AABW. Compared to dense shelf water production, open ocean convection is a relatively minor and potentially infrequent contributor to AABW formation (e.g., Gordon 2001). The different mechanisms involved in AABW formation (open ocean convection or dense shelf water production) may also respond differently to a changing climate. To encompass the complete range of AABW volume and property responses, the influence on each process must be evaluated. This study provides evidence of how shelf water–sourced AABW responds to changing surface buoyancy fluxes as a result of a warming atmosphere and increased surface freshwater fluxes.

Observed freshening of AABW (Aoki et al. 2005; Rintoul 2007; Purkey and Johnson 2010, 2013) is linked with evidence of increased precipitation and glacial melt around Antarctica (e.g., Jullion et al. 2013). AABW observations also indicate a warming and contraction of the densest water mass (Purkey and Johnson 2010, 2013). Warming of AABW remains a significant contributor to sea level rise through thermosteric effects (Purkey and Johnson 2010), while increases in glacial runoff have been shown to enhance sea level rise within the Southern Ocean (Rye et al. 2014; van den Berk and Drijfhout 2014). AABW property and volume changes will likely alter the global overturning circulation. Current studies often refer to the role of AABW in the ''bipolar seesaw.'' Under such a scenario, reduced AABW transport enhances North Atlantic Deep Water (NADW) circulation (e.g., England 1993; Seidov et al. 2001; Martin et al. 2015), which may drive systemwide changes (e.g., Seidov et al. 2001). Despite the many studies undertaken investigating AABW sensitivity to forcing, a complete understanding of the role AABW plays in the global climate system remains uncertain.

Previous modeling studies investigating the sensitivity of AABW to freshwater fluxes focus on a uniformly distributed surface freshwater flux over the Southern Ocean, simulating either changes in precipitation, ice-melt, or ice-sheet runoff and/or collapse (e.g., Aiken and England 2008; Trevena et al. 2008; Swingedouw et al. 2009; Menviel et al. 2010; Kirkman and Bitz 2011; Ma and Wu 2011; Bintanja et al. 2013, 2015; Morrison et al. 2015). However, changes to freshwater fluxes across Antarctica are not necessarily uniformly spread over the Southern Ocean. Increased basal melting of glacial ice sheets represents a significant local freshwater source derived solely at the continental edge. Such melting is suggested to result from increased intrusions/transport of warm CDW onto the continental shelf (e.g., Thoma et al. 2008; Jacobs et al. 2011). Changes in CDW volume and circulation on the shelf may be attributed to changes in the westerly winds around Antarctica as a result of anthropogenic forcing (Thoma et al. 2008; Dinniman et al. 2011, 2012); however, a complete understanding of the mechanisms driving increased basal melt remains uncertain (Dinniman et al. 2012). While changes in basal melt are most prominent in West Antarctica (e.g., Jacobs et al. 2011; Joughin et al. 2012; Pritchard et al. 2012), changes in East Antarctic ocean circulation and properties may also indicate increased basal melting (Khazendar et al. 2013; Gwyther et al. 2014).

Changes to atmospheric heat fluxes and their resulting contribution to surface buoyancy and AABW properties have remained relatively neglected. Despite the sea surface cooling response simulated from anthropogenic forcing (as a result of a strengthened halocline hindering the upwelling of warm deep waters to the surface; refer to section 3a; Trevena et al. 2008; Swingedouw et al. 2009; Ma and Wu 2011), changes in surface heat fluxes remain an important component of any buoyancy adjustment. Increases in net radiative fluxes under climate change are dominated by an increase in downward longwave radiation (DLR; Stephens et al. 2012; Zelinka and Hartmann 2012). Surface atmospheric sensible heat changes also act as a major influence over the Southern Ocean (Taylor et al. 2013). Such heat flux changes, while having the potential to alter surface water buoyancy, may also promote glacial ice melt and reduce sea ice formation. All such changes may result in adjustments to the convective mixing on the shelf and open ocean and hence the resulting AABW formation and properties.

Within an idealized ocean-only sector model, Morrison et al. (2015) show that both a latitudinally independent and a Southern Hemisphere–only atmospheric warming may lead to sea surface cooling and freshening trends in the Southern Ocean. Zhang (2007) investigates changes to Antarctic sea ice within a coarse-resolution ocean–ice model following increases in surface air temperature (SAT), DLR, precipitation (P), and decreases in downward shortwave radiation (following trends in the NCEP–NCAR reanalysis data). They find that increases in SAT and DLR play a key role in influencing decadal trends in sea ice production (and hence brine rejection).

Our study quantifies the influence of both freshwater and heat flux changes to the surface buoyancy and shelf properties and how they independently contribute to the transient responses of AABW formation and water mass properties. We evaluate how changes to glacial runoff, confined to sources around the Antarctic coast, alter AABW circulation and properties and compare the response to increases in precipitation. We also investigate the sensitivity of Antarctic shelf waters, AABW properties, and overturning circulation to

increased SAT and DLR. Our results provide an indication of the relative importance and contribution that heat fluxes have in controlling AABW formation and properties. Analysis is performed within a 0.25° eddy-permitting sector model, where realistic bathymetry and surface forcing is applied (Snow et al. 2015). The sector model, with ocean–ice coupling, allows us to evaluate the response of shelf-sourced AABW to buoyancy changes, providing a new range of responses absent from many previous modeling studies that rely solely on open ocean convection to form AABW (e.g., Heuzé et al. 2015). An increased understanding of the role of buoyancy flux changes around Antarctica will allow for an improved interpretation of how these relative changes influence AABW and the role AABW plays in the changing climate.

2. Method

a. Model

Most previous modeling studies evaluating the effect of buoyancy flux changes around Antarctica have generally been performed with coarse ocean resolutions, where eddy contributions to the circulation must be parameterized (with a few exceptions; e.g., Morrison et al. 2011, 2015). Changing from coarse to eddy-permitting resolution leads to improvements in the modeled representation of the Southern Ocean meridional overturning circulation (Spence et al. 2009) as well as improved abyssal ocean heat uptake (Zhang and Vallis 2013). Hence, applying eddy-permitting resolution may provide improved representation of the dynamical impacts evolving from buoyancy flux changes not represented at coarse resolution. In this study, a realistic bathymetry sector model of the Atlantic Ocean is used for a suite of sensitivity experiments into the dependence of AABW formation and properties on buoyancy surface forcing [see Snow et al. (2015) for full details on the development of this model]. We increase the horizontal resolution of the model described by Snow et al. (2015) to 0.25° on a Mercator grid, with 65 vertical levels increasing from a thickness of 5 m at the surface to 200 m at depth.

The Atlantic Ocean is chosen as the sector domain as it includes formation regions for both AABW and NADW and hence allows for representation of the upper and lower global overturning cells. The sector is generated from a combination of the NOAA/GFDL 0.25° global bathymetry (Delworth et al. 2012) and the Weddell Sea coast of the ETOPO2v2 globally gridded 2′ ocean and land topography (NOAA 2001). The boundaries are defined to include the entire Atlantic Ocean, with zonally reentrant boundary conditions at

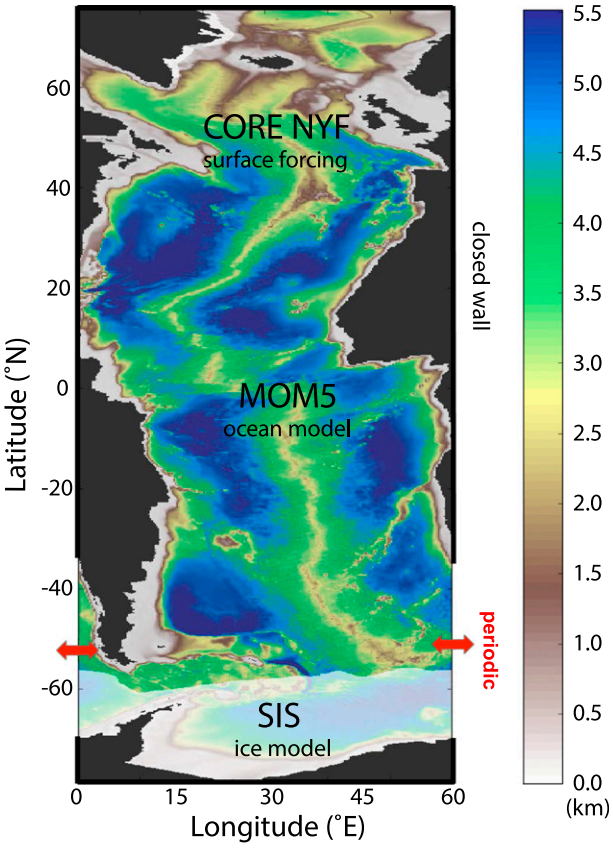

FIG. 1. Summary of the model domain, boundary condition configuration, and forcing/model components.

Drake Passage latitudes to permit a representative Antarctic Circumpolar Current (ACC) flow. Within these boundaries the domain is deformed laterally to fit a 60°-wide sector with matching conditions set at the periodic boundaries (Fig. 1). The Modular Ocean Model, version 5 (MOM5; Griffies 2012), provides the ocean component of the model and is coupled to the GFDL sea ice simulator (SIS; Winton 2000). Version 2 of CORE phase 2 (CORE2v2) normal year forcing (NYF; Large and Yeager 2009) is applied to the surface with the deformation of the forcing fields equivalent to that of the bathymetry in order to maintain constancy between ocean and land forcing (Snow et al. 2015). The CORE fields provide the surface wind and buoyancy forcing component of the model. It is through perturbations to these fields that the buoyancy flux changes are applied. Vertical mixing is achieved through the K profile parameterization (KPP) surface boundary layer scheme of Large et al. (1994), an interior gravity wave mixing scheme (Simmons et al. 2004) and a coastal tidal mixing scheme (Lee et al. 2006). No overflow parameterization is applied because Snow et al. (2015) shows that such parameterizations do not significantly improve AABW overflow

representations. At 0.25° resolution, we do not employ an eddy parameterization but do apply the Fox-Kemper et al. (2008) parameterization of submesoscale eddies.

The ACC transport (102 Sv; 1 Sv $\equiv 10^6\,m^3\,s^{-1}$) and the NADW overturning (4.5 Sv; Fig. 1) are relatively weak compared to observations (e.g., the ACC is 137 ± 7 Sv; Meredith et al. 2011). These low values result from the incomplete process representation (such as including only one-sixth of the globe in our domain and the closed wall boundaries at the northern edge). However, the goal of our model is to provide a representation of the circulation present in the global ocean, including that of the lower and upper cells, and the key processes defining AABW. Marginally lower ACC and NADW compared to observations does not hinder our reproduction of the overall processes defining AABW. Further, since our analysis is undertaken relative to a control state, any small differences in the magnitudes of the circulation cells do not necessarily influence the processes governing change in the perturbation runs.

Many previous studies of the influence of buoyancy flux changes on AABW have been coupled to an atmospheric model (e.g., Aiken and England 2008; Ma and Wu 2011) such that the role of changing surface buoyancy fluxes are not independent from other atmospheric changes (i.e., subsequent induced wind shift/intensification). In this study, surface forcing perturbations are applied as a step change to the CORE forcing, removing any such atmospheric feedback and allowing for a mechanistic understanding of how each buoyancy flux and forcing term independently influences the AABW formation and properties.

b. *Buoyancy perturbations*

In this section we outline the formulation of buoyancy flux changes that are consistent with future projections based on the CMIP5 representative concentration pathways (RCPs). The application of heat and freshwater fluxes are considered separately with a range of values applied in order to capture the relative influence of each buoyancy term.

1) HEAT FLUXES

Heat flux changes are applied through a contribution of DLR and SAT. To quantify possible future projections of DLR and SAT in the Southern Ocean, outputs from 15 CMIP5 models are analyzed (Figs. 2a–d). The DLR and SAT in each model are zonally averaged over the ocean, and the differences between the present-day mean (2006–16) and the projected decadal mean (2090–2100) are calculated for two RCPs—RCP4.5 and RCP8.5 (corresponding to top-of-the-atmosphere imbalances of 4.5 and 8.5 $W\,m^{-2}$, respectively, by 2100; Taylor et al. 2012). The forcing perturbation is based on the multimodel mean, except that, since we are primarily interested in the sensitivity of AABW, changes in DLR and SAT north of 50°N are kept constant in order to avoid northern polar amplification dominating the model response. The perturbations in DLR and SAT are then added to the CORE2v2 fields (Figs. 3a,b) as a latitudinally invariant field for each of the RCP4.5 and RCP8.5 cases (experiments labeled H45 and H85). To attain a wider spectrum of possible responses (and as a result of the limited model output available for RCP2.6 and RCP6.0), we average the H45 and H85 forcing to obtain a representative RCP6.0 case (labeled H60) and halve the H45 input to attain a fourth minimum warming scenario (labeled H20). Table 1 provides a summary of the heat flux perturbation experiments.

Averaged over 100 years of simulations, the induced step changes correspond to a domain-averaged increase in DLR of 0.085 $W\,m^{-2}\,yr^{-1}$ for RCP4.5 and 0.21 $W\,m^{-2}\,yr^{-1}$ for RCP8.5. These values provide similar trends to observations; Zhang (2007) estimates that the trend in DLR from 1979 to 2004 is 0.069 $W\,m^{-2}\,yr^{-1}$ over the Southern Ocean based on reanalysis data, while Stephens et al. (2012) indicates a current global change of 0.18 $W\,m^{-2}\,yr^{-1}$ over the ocean within ±60° of the equator. Reanalysis data indicates a current Southern Ocean increase in SAT of 0.027°C yr^{-1} from 1979 to 2004 (Zhang 2007). Our simulations provide a step change that over 100 years averages to an increase in SAT of 0.014°C yr^{-1} for RCP4.5 and 0.033°C yr^{-1} for RCP8.5.

2) FRESHWATER FLUXES

Changes in the freshwater budget of the Southern Ocean are likely to be derived from a combination of glacial runoff from Antarctica and trends in precipitation (as well as the response of sea ice). Antarctic glacial melt from ice sheets has increased significantly over recent decades (e.g., Jacobs et al. 2011; Pritchard et al. 2012) from 30 Gt yr^{-1} in 1992–2001 to 147 Gt yr^{-1} in 2002–11 (IPCC 2013), while total increases in Antarctic melt (also including thinning of floating shelves) is estimated at 350 Gt yr^{-1} over the past 20 years (Rye et al. 2014). The CORE2v2 Antarctic runoff equates to 397 Gt yr^{-1} mass flux within our domain (total Antarctic runoff is estimated at approximately 2500 Gt yr^{-1}; Large and Yeager 2009; we remind the reader that our domain is only about one-sixth that of the globe). There is no direct estimates of future glacial runoff changes; hence, we elect to amplify the existing runoff pattern. To simulate the enhanced runoff, we apply increases of 1.3, 1.6, 2, and 2.3 times to the CORE2v2 runoff sourced from the Antarctic coastline (experiments defined as R13, R16, R2, and R23, respectively; Fig. 3b; Table 1). The

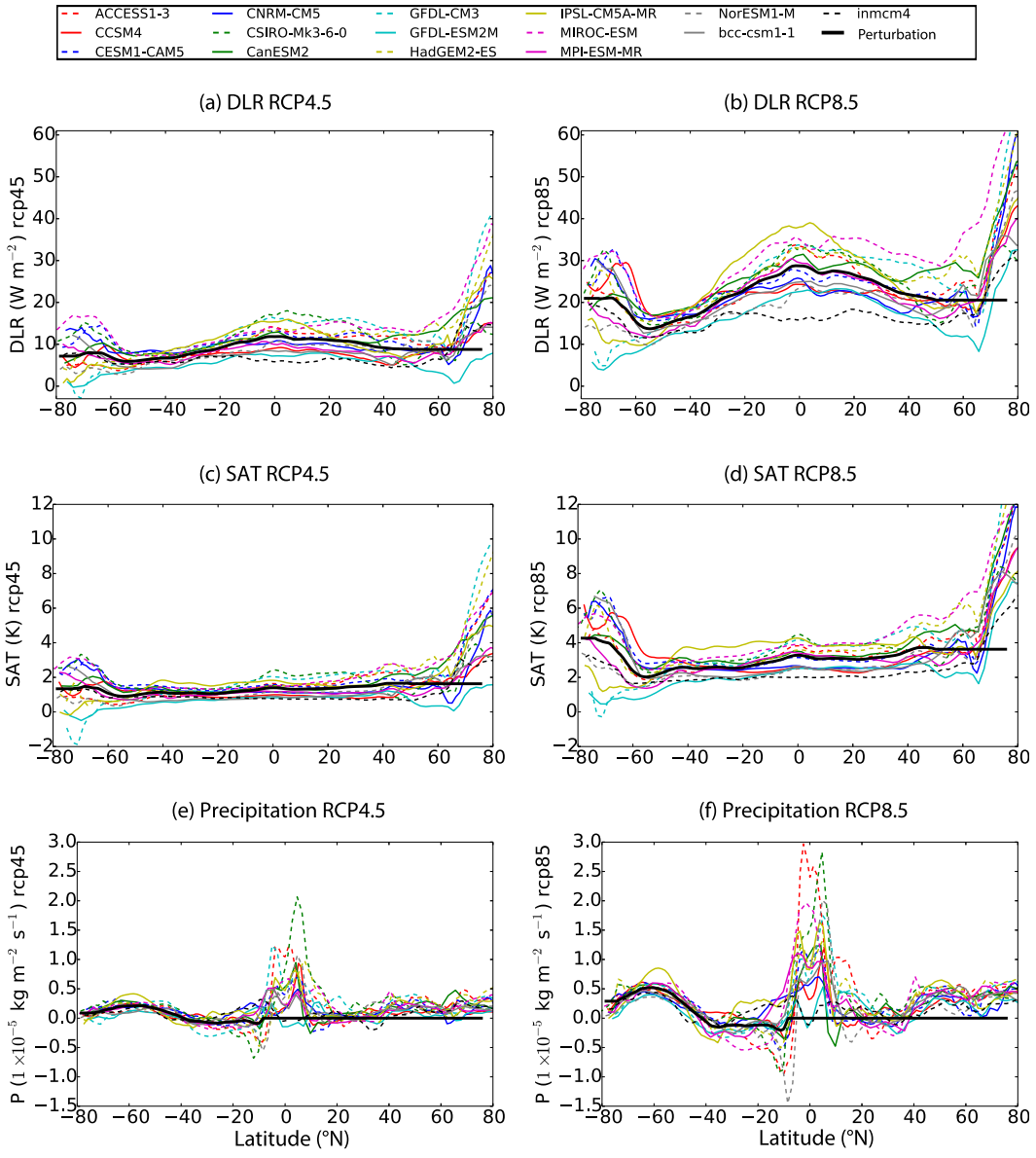

FIG. 2. Difference in the decadal averages from 2006–16 to 2090–2100 for zonally averaged over-ocean DLR (W m^{-2}) in the (a) RCP4.5 and (b) RCP8.5 forcing scenarios; zonally averaged over-ocean SAT (°C) for (c) RCP4.5 and (d) RCP8.5; and precipitation (10^{-5} kg m^{-3} s^{-1}) for (e) RCP4.5 and (f) RCP8.5 across 15 different CMIP5 models. The thick black line is the applied perturbation of the multimodel average south of 40°N for DLR and SAT and south of 10°S for precipitation of each CMIP5 model shown, interpolated to the Atlantic sector model latitudes.

coastally uniform distribution of the CORE2v2 runoff does not allow for regional variability of basal melt rates (van den Berk and Drijfhout 2014); however, it still provides an indication of how glacial runoff changes may influence shelf properties.

In parallel to the runoff cases, we also investigate scenarios in which precipitation increases south of approximately 10°S (chosen because this is the latitude of minimum cumulative freshwater flux change, based on the CMIP5 multimodel mean; Figs. 2e,f). Our model allows no net mass increase of the ocean. Excess mass from changes in precipitation, evaporation, and runoff is removed by adjusting the precipitation using a constant offset. We aim to minimize this offset by inducing changes only to 10°S, where the minimum change in precipitation is attained in the perturbation. Further, since we are focused on the Southern Hemisphere response to buoyancy flux changes, changes to Northern Hemisphere fluxes are ignored. We consider two precipitation experiments, P45 and P85, which apply the

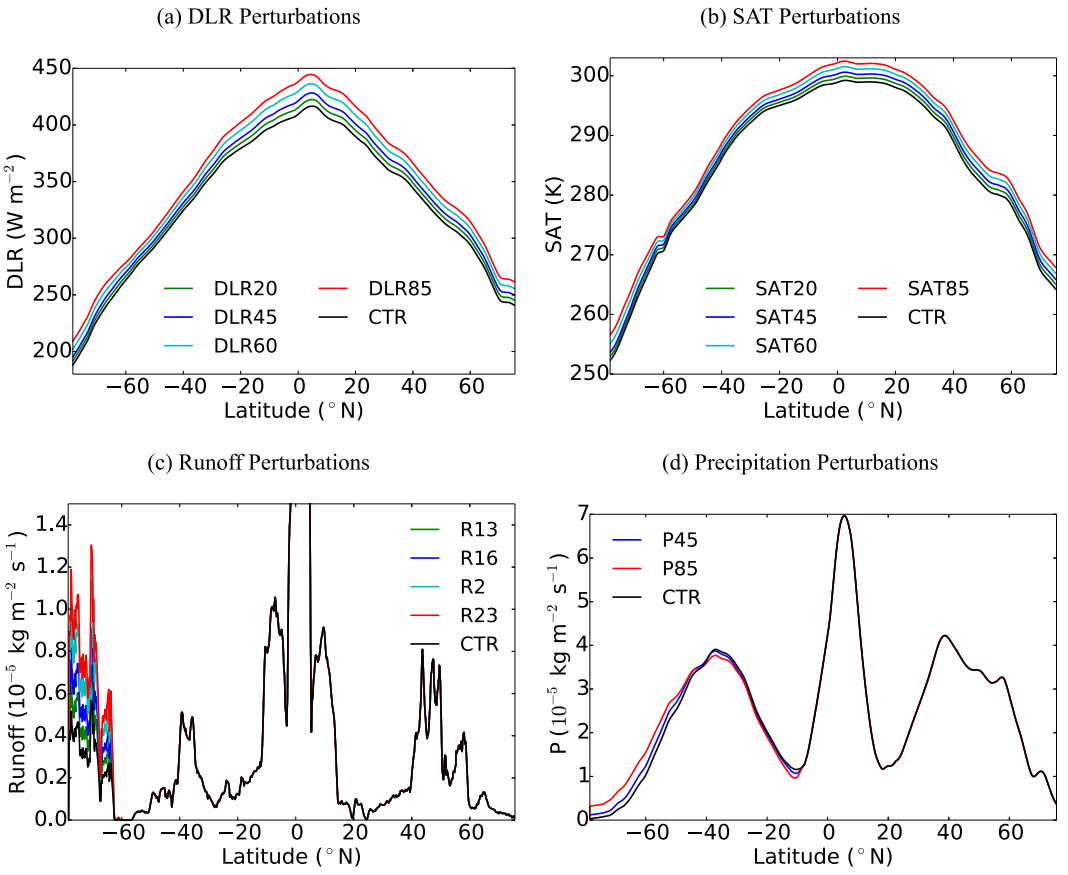

FIG. 3. Zonally averaged CORE2v2 (black lines; CTR) (a) DLR, (b) SAT, (c) runoff, and (d) precipitation, along with the zonally averaged perturbation experiments (colored lines). Perturbations include heating scenarios H20, H45, H60, and H85; freshwater perturbations of runoff R13, R16, R2, and R23; and freshwater perturbation of precipitation P45 and P85.

expected latitudinally averaged precipitation changes (the projected 2090–2100 mean from the 2006–16) across the ocean in the RCP4.5 and RCP8.5 scenarios from a 15-model mean (Figs. 2c,d and 3d).

c. *Experiments*

The control state (CTR) is spun up for 500 years (Fig. 4), maintaining the original CORE2v2 NYF fields. At year 501 perturbation experiments are branched from the control run. A total of four runoff, two precipitation, and four heating perturbation experiments are performed (Table 1). Each perturbation run is continued for 100 years, and the transient response of each experiment is compared with the equivalent period in CTR to quantify AABW's sensitivity to each buoyancy flux change.

d. *Net surface buoyancy flux*

One caveat regarding the freshwater fluxes is the influence of salinity restoring. Salinity restoring is commonly applied to ocean models to maintain an equilibrium surface salinity in close agreement with observations. In the Atlantic sector, salinity restoring is applied to the ocean surface with a damping time scale

TABLE 1. Summary of perturbation experiments undertaken for each of the freshwater flux (FW) and heat flux (HF) simulations. The relative freshwater or heat flux component influenced is given in column 3, with information on the RCP used to derive the magnitude of change provided.

Run	Flux change	Flux component	RCP
R13	FW	1.3 times runoff	—
R16	FW	1.6 times runoff	—
R2	FW	2.0 times runoff	—
R23	FW	2.3 times runoff	—
P45	FW	Precipitation	RCP4.5
P85	FW	Precipitation	RCP8.5
H20	HF	SAT + DLR	0.5 times RCP4.5
H45	HF	SAT + DLR	RCP4.5
H60	HF	SAT + DLR	0.5 (RCP4.5 + RCP8.5)
H85	HF	SAT + DLR	RCP8.5

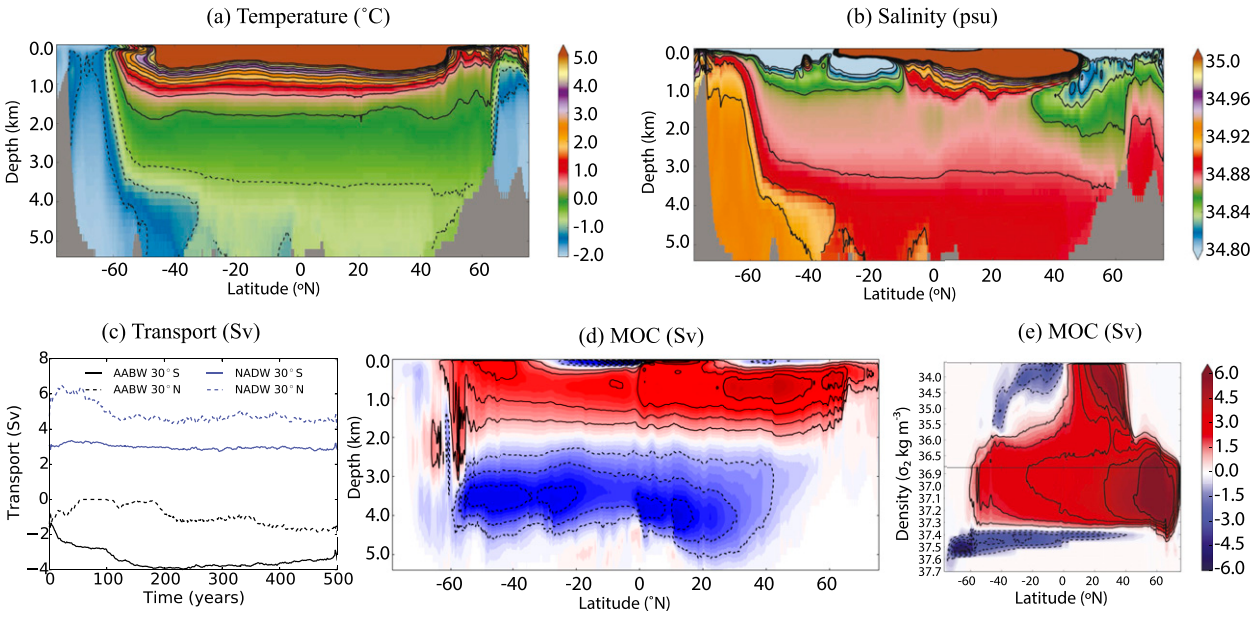

FIG. 4. Model control state (averaged over years 490–500) of (a) zonally averaged temperature (°C), with contours at 0.5°C intervals, (b) zonally averaged salinity with contours at 0.04-psu intervals, (c) evolution of AABW and NADW transports at 30°S and 30°N (evaluated as the minimum and maximum, respectively, of the MOC at densities greater than $\sigma_2 = 36.8\,\mathrm{kg\,m^{-3}}$), and MOC in (d) depth space and (e) σ_2 space (Sv) with contours at 1-Sv intervals (excluding 0 Sv).

of 60 days. With the restoring component, the total freshwater flux F_{fw} ($\mathrm{kg\,m^{-2}\,s^{-1}}$) into the ocean is given by

$$F_{\mathrm{fw}} = F_p - F_e + F_{\mathrm{runoff}} + F_{\mathrm{melt}} + F_{\mathrm{rest}}, \tag{1}$$

where F_p is the freshwater flux from precipitation, F_e is the flux from evaporation, F_{runoff} is the freshwater flux from runoff, F_{melt} is the flux from ice melt and formation, and F_{rest} is the flux from salinity restoring. The restoring term partly counters the applied freshwater flux perturbations (e.g., in the R2 case, salinity restoring reduces the freshwater flux change by approximately one-third). However, since we account for the salinity restoring changes in our freshwater flux calculation and are only concerned with the total change in freshwater fluxes in our analysis, the damping by the salinity restoring does not influence our results.

An initial adjustment period of approximately 10 yr occurs where the model responds to the perturbed runoff or precipitation and the equivalent freshwater flux applied through salinity restoring responds (not shown). After this period, an approximately steady trend to the freshwater flux is maintained.

Similarly to the freshwater fluxes, the total heat flux F_h ($\mathrm{W\,m^{-2}}$) is defined as follows:

$$F_h = F_{\mathrm{sw}} + F_{\mathrm{lw}} + F_{\mathrm{lat}} + F_{\mathrm{sens}}, \tag{2}$$

where F_{sw} is the heat flux from shortwave radiation, F_{lw} is the flux from incoming minus outgoing longwave radiation, F_{lat} is the latent heat flux, and F_{sens} is the sensible heat flux. The freshwater and heat fluxes are combined to produce a net surface buoyancy flux (B_{net}; $\mathrm{m^2\,s^{-3}}$):

$$B_{\mathrm{net}} = g\alpha\frac{F_h}{\rho_0 c_p} + g\beta\frac{F_{\mathrm{fw}}S_0}{\rho_{\mathrm{fw}}}, \tag{3}$$

where g is the acceleration due to gravity ($9.81\,\mathrm{m\,s^{-2}}$), α is the thermal coefficient of expansion, $\rho_0 = 1035\,\mathrm{kg\,m^{-3}}$ is the density of seawater, $c_p = 992.1\,\mathrm{J\,kg^{-1}\,°C^{-1}}$ is the specific heat capacity of seawater, β is the haline contraction coefficient, S_0 is the surface salinity, and $\rho_{\mathrm{fw}} = 1000\,\mathrm{kg\,m^{-3}}$is the density of freshwater. The average change in net surface buoyancy flux south of 60°S is used to provide a comparative measure of the influence of each perturbation and to indicate the role buoyancy plays in controlling AABW properties.

3. Results

a. *Surface and sea ice response*

During the latter stages of the model spinup (simulated with CTR parameters) there is no systematic trend in the annual cycle of the sea ice. When the heat flux forcing is perturbed, sea ice adjusts rapidly within the

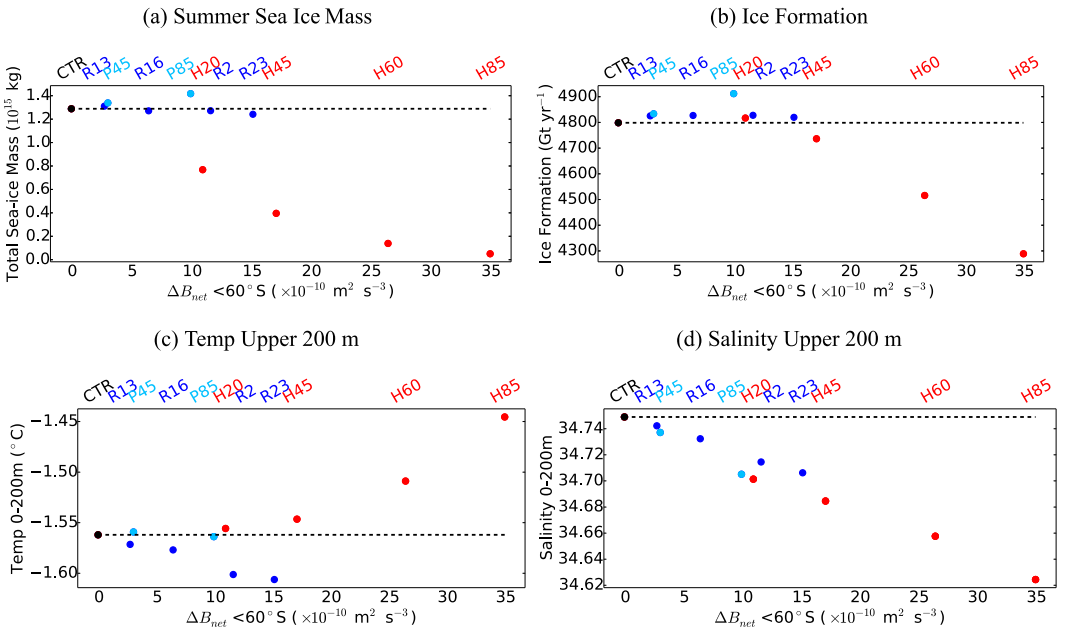

FIG. 5. Total (a) summer sea ice mass (10^{15} kg) and (b) freshwater flux (Gt yr^{-1}) leaving the ocean as a result of ice formation south of 40°S, and (c) upper-ocean temp (0–200 m) and (d) upper-ocean salinity (0–200 m) south of 50°S for each of the heating (red) and freshwater (blue) perturbations averaged over the last 10 years of the simulations with respect to change in net buoyancy flux of each perturbation. Dashed line shows the value of CTR. Details of the precipitation, runoff, and heat flux perturbations are given in Table 1.

first few years of the perturbation (not shown). A substantial decrease in total summer sea ice mass south of 60°S occurs for all heat flux perturbations, almost disappearing in summer for the H85 case (Fig. 5a). This decrease occurs despite unchanged ice formation rates in the H20 case (Fig. 5) due to increased melt rates over the summer months.

The sea ice mass change is negligible for increasing freshwater fluxes from runoff; however, sea ice mass increases by up to 10% for the precipitation cases (Fig. 5; P85). No trend in the snow-to-ice mass flux was found (not shown), and hence the reason for the increased sea ice in P85 compared with R2 (which have similar change in net buoyancy flux) may be understood by the broadly distributed nature of the flux change in P85 relative to the coastally confined runoff of R2. R2 drives local changes on the shelf but does not influence the larger Southern Ocean region as P85 does. The increased sea ice in P85 (relative to CTR) occurs because freshwater freezes at a higher temperature than saline water (freezing point is −1.8°C at the surface); surface freshening across the Southern Ocean increases sea ice growth.

An alternative measure of the sea ice response is the annual freshwater flux from ice formation, which also decreases with increasing surface heat flux, though a modest increase occurs for the freshwater flux perturbations (Fig. 5b). Given that the system adjusts to the perturbations rapidly, the amount of formation indicates the magnitude of the seasonal cycle. The decrease in annual sea ice formation in warming cases thus indicates that both summer and winter sea ice have decreased, while the small, but systematic, increase (0.5%–2%) in production in the freshwater scenarios is consistent with a lower barrier to sea production in fresher water (Fig. 5b; runoff and precipitation perturbations). The exception to the trends is that of H20. In that case the ice formation does not change significantly from CTR despite the warming. The unchanged formation rate may be a result of the decreased surface salinity (Fig. 5d) allowing favorable ice formation conditions that compensate the warmer atmospheric conditions inhibiting ice formation. In the H45–H85 cases, the increased heat flux overwhelms the influence of surface freshening to hinder ice formation.

A total reduction in sea ice mass (Fig. 5a) facilitates an increase in freshwater flux to the ocean from sea ice melt. Following the reduction in sea ice, a net reduction in ice melt (and formation) occurs (Fig. 5b). Since ice formed in the southern regions of the Southern Ocean is often advected northward (by winds and ocean surface Ekman transport), reduced ice formation leads to a decreased northward flux of freshwater from sea ice.

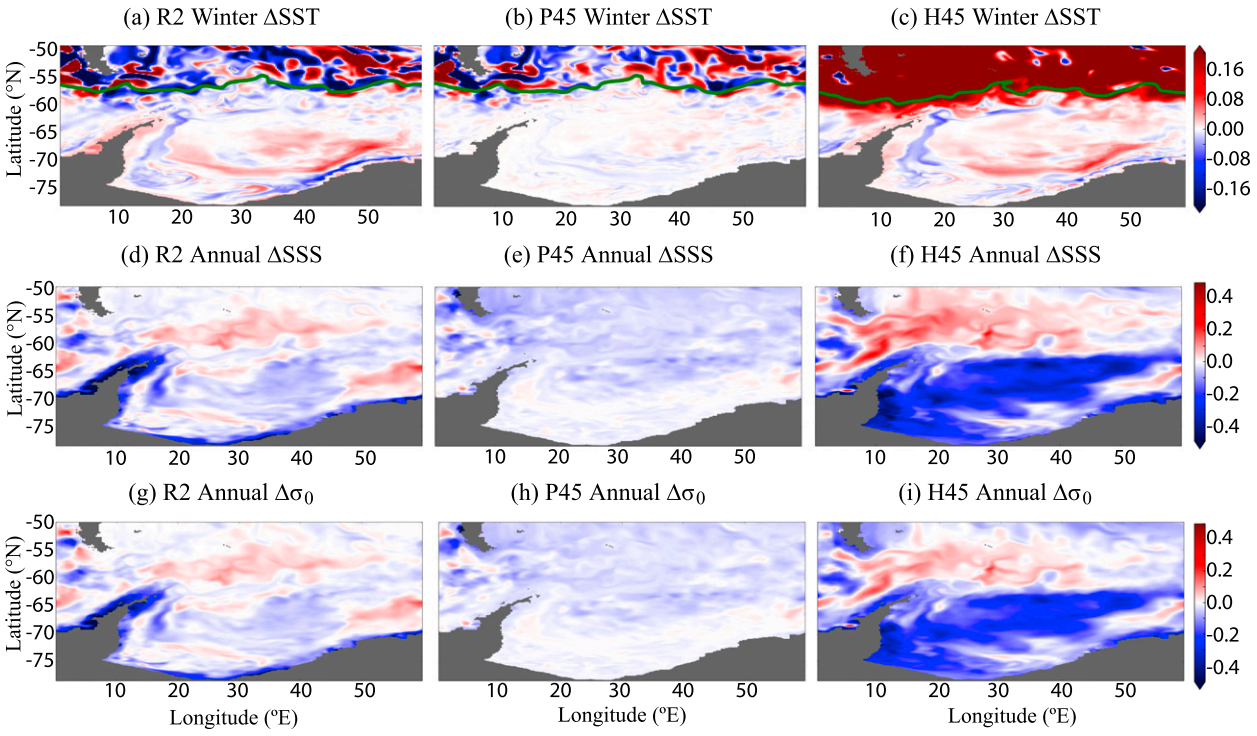

FIG. 6. Years 90–100 difference from CTR in (a)–(c) winter SST (°C), (d)–(f) annual sea surface salinity (SSS), and (g)–(i) σ_0 (kg m^{-3}) for (left)–(right) R2, P45, and H45, respectively. Green contours in (a)–(c) show the defining boundary of winter sea ice extent between winter SST changes of different magnitudes.

Further, since ice formation is a net freshwater sink while melt is a source, the decreased formation rate allows a relative increase in freshwater fluxes south of 65°S (9.8×10^{-10} m^2 s^{-1} for H45 over the final decade), while the decreased northward flux (and hence decreased melt) in the northern regions leads to a net freshwater flux decrease between 50° and 65°S (by -6.7×10^{-10} m^2 s^{-1} for H45 over the final decade). The resultant freshwater flux change occurring via ice removal south of 65°S is an order of magnitude larger than that induced by applying projected precipitation changes (e.g., P45 leads to a freshwater flux change south of 60°S of 2.8×10^{-10} m^2 s^{-1} over the final decade). These results emphasize the importance of sea ice and heat fluxes in controlling the buoyancy changes within the Southern Ocean. Since sea ice mass decreases with increased heating, surface freshening concurrently increases. Such increases are in contrast to Morrison et al. (2015); however, their study did include sea ice and so was unable to incorporate the surface freshwater flux feedback mechanism.

Annually averaged upper-ocean temperature warms significantly across the Southern Ocean south of 60°S under the heating experiments (Fig. 5c). Freshwater fluxes on the other hand lead to upper-ocean cooling. This cooling is likely a result of increased surface freshwater fluxes strengthening the upper-ocean halocline and impeding the convection that precedes AABW formation (Aiken and England 2008; Trevena et al. 2008; Swingedouw et al. 2009; Ma and Wu 2011). Reduced convection increases the residence time of surface waters under atmospheric fluxes, facilitating a net cooling.

Despite the upper-ocean warming under heating, winter SST illustrates regions of cooling on the shelf (Fig. 6c). The shelf cooling is more widespread in the runoff case (Fig. 6a). This cooling trend may be explained through changes in on-shelf/off-shelf exchange (see section 3b) as a result of decreased shelf water density (Figs. 6g,i). The precipitation experiments exercise less influence on the shelf water properties as a result of the persistent ice barrier near the shelf insulating the ocean from the atmospheric fluxes. Hence, the precipitation experiments lead to the least reduction in on-shelf density (e.g., at the surface; Fig. 6b), the smallest changes in the on-shelf/off-shelf exchange (section 3b), and consequentially the smallest shelf cooling response in regions of AABW source waters (which in this model occurs on the eastern edge of the shelf).

The reduction in sea ice and increase in upper-ocean temperature for all the warming cases (Figs. 5a,c) is in contrast to recent observations showing increased ice production around Antarctica (Parkinson and Cavalieri 2012; Bintanja et al. 2013; Turner et al. 2013; Blunden et al. 2014) and an ongoing cooling trend of Southern Ocean surface waters (e.g., Latif et al. 2013; Fan et al. 2014). Mechanisms driving these observed trends are poorly understood. Decreased Southern Ocean SST may be attained through a feedback between oceanic convection and AABW formation around Antarctica. Increased heat and freshwater fluxes increase the strength of the upper-ocean stratification, hindering the onset and strength of deep convection and hence the flux of warm waters brought to the surface. Indeed, many modeling studies simulating increased surface freshwater fluxes around Antarctica produce cooling of surface waters (Aiken and England 2008; Trevena et al. 2008; Swingedouw et al. 2009; Ma and Wu 2011; Bintanja et al. 2013, 2015; Morrison et al. 2015). While our results produce no significant change in SST as a result of increases in runoff and precipitation (not shown), the upper 200 m does illustrate a cooling trend for the runoff cases (Fig. 5c).

Morrison et al. (2015) found surface cooling responses in the Southern Ocean as a result of atmospheric warming, though such cooling only occurred for small increases in surface heat flux that allowed a feedback upon surface freshening, while for larger heat fluxes, SST warming occurred. The latter result agrees with Zhang (2007), who found increasing upper-ocean temperatures as a result of increased SAT and DLR. In our analysis, the heating scenarios increase upper-ocean temperatures south of 60°S in all cases. The reduction in convective heat flux in our experiments (i.e., reduction of surface mixing with interior warm CDW) resulting from increased surface stratification does not compensate the surface warming. For example, the maximum decrease in convective heat flux over the perturbation period for H45 is of the order $0.3\,\mathrm{W\,m^{-2}}$. However, for the last decade of the experiment (when increased SST will reduce the relative heat flux from longwave and sensible heating) a change in heat flux (relative to CTR) of $1.4\,\mathrm{W\,m^{-2}}$ to the ocean surface south of 40°S is maintained.

Finally, the observed cooling of SST around Antarctica is postulated to be only an initial response to atmospheric changes and may indeed lead to warming in future periods (Marshall et al. 2014; Ferreira et al. 2015). The role of internal variability in the current observations also remains unclear (Zunz et al. 2013). It has been proposed that these recent observational trends may in fact originate from internal variability on decadal to centennial time scales (Martin et al. 2013; Latif et al. 2013; Zunz et al. 2013; Fan et al. 2014) rather than external anthropogenic influences.

b. *Shelf and deep ocean response*

While surface changes are an important component of the climate response, this study is primarily designed to examine the influences on AABW properties. Freshening of both shelf (waters shallower than 1000 m and south of 60°S) and AABW water masses (Figs. 7d–f) is consistent with observational evidence (e.g., Zenk and Morozov 2007; Purkey and Johnson 2010; Hellmer et al. 2012; Azaneu et al. 2013). Freshening of shelf waters is greatest in the warming scenarios because of the dominant role ice removal has in the freshwater flux budget. Precipitation cases, on the other hand, produce the smallest change in shelf salinity since it exerts minimal influence over the ice-covered shelf (see section 3a).

All simulations produce a widespread warming trend in the deep ocean (Figs. 7a–c and 8, left). The warming in the freshwater cases is likely in response to the reduced convection from increased surface freshening and stronger stratification. Convection mixes cold surface water downward; thus, reduced convection results in an overall subsurface warming. The warming is enhanced in the precipitation case compared to runoff (Fig. 8, left), likely due to the minimal influence runoff has on the open ocean (and hence the open ocean convection) compared to precipitation. The warming is amplified in the heating scenarios (as expected), with the magnitude of the warming being proportional to the size of the heat flux perturbation (Fig. 8, left).

The warming trends of deep water are in accordance with observations (Robertson et al. 2002; Fahrbach et al. 2004; Purkey and Johnson 2010; Fahrbach et al. 2011). However, a striking response of the runoff cases (Figs. 7a and 9a) and initial years of the warming and precipitation cases (not shown) is a cooling of the densest bottom waters north of 60°S. This cooling can be traced back to AABW sources on the shelf, which decreases in temperature during winter (Figs. 6a–c, 7a–c, and 8, right) and is advected to the ocean bottom within the first decade (Fig. 10). As the densest source of AABW, the cool shelf waters descend to the abyssal ocean creating regions of cooling on the ocean bottom despite warming within the deep ocean.

The cooling of dense shelf waters occurs in response to reduced on-shelf/off-shelf exchange (Fig. 11). As the density of the shelf water decreases (Figs. 6 and 7), off-shelf flow is diminished, hindering the on-shelf exchange flow. A similar result was found by Stewart and Thompson (2015), in which decreased surface salt fluxes within a highly idealized slope configuration decreased

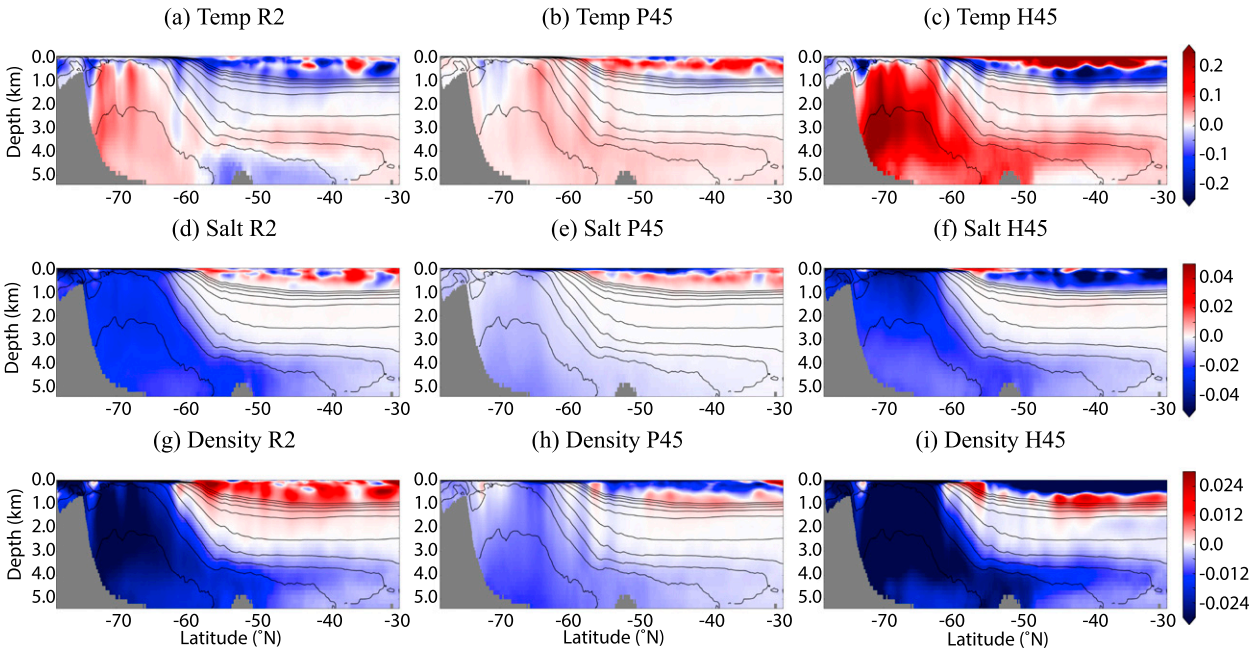

FIG. 7. Perturbation minus CTR in zonally averaged (a)–(c) temperature (°C), (d)–(f) salinity, and (g)–(i) potential density referenced to 2000 m (σ_2; kg m^{-3}) averaged over the last decade of the perturbation experiments for (left)–(right) cases R2, P45, and H45, respectively. Contours show the density levels of CTR zonally averaged over the last decade of the run from 37.1 to 37.65 at intervals of 0.05 kg m^{-3}.

AABW off-shelf flow and CDW on-shelf flow. Since the waters flowing onto the shelf are derived from the relatively warm CDW (Fig. 4), reduced exchange leads to cooling on the shelf from where AABW is derived (Figs. 6 and 7). The mechanism active in this model is therefore consistent with recent evidence of cooling of dense shelf water across Antarctica from 1958 to 2010 (Azaneu et al. 2013). Our results provide the first evidence of a positive feedback on dense shelf water cooling via changes in the on-shelf/off-shelf exchange flow.

The different abyssal cooling responses between the schemes are due to the contrasting ways the buoyancy flux components influence the shelf versus the open ocean. Precipitation produces the weakest cooling response on the shelf, yet enhanced deep ocean warming (Fig. 8). Such responses are likely a result of the limited impact precipitation has on shelf densities compared to the other perturbations [Figs. 7b, 8 (right), and 9b] due to precipitation fluxes being more dispersed across the Southern Ocean and the persistent ice barrier near the shelf insulating the ocean surface from atmospheric changes. With limited density changes there is minimal influence on the on-shelf/off-shelf exchange flow compared to the other experiments (Fig. 11). Hence, precipitation dominantly drives changes in the open ocean, leading to an overall warming of the abyssal ocean through most of the perturbation period (Fig. 12).

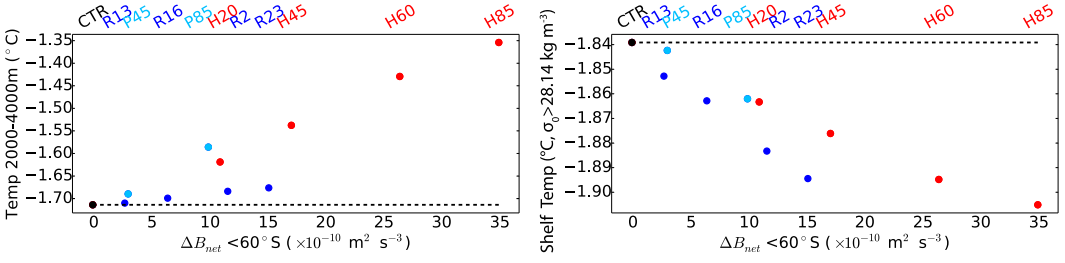

FIG. 8. (left) Deep ocean temperature (2000–4000 m) and (right) dense shelf water temperature (taken as the temperature of waters denser than the mean CTR winter density; σ_2 = 28.14 kg m^{-3}) south of 60°S for each of the heating (red) and freshwater (blue) perturbations averaged over that last 10 years of the simulations with respect to change in net buoyancy flux of each perturbation. Dashed line shows the value of CTR. Details of the precipitation, runoff, and heat flux perturbations are given in Table 1.

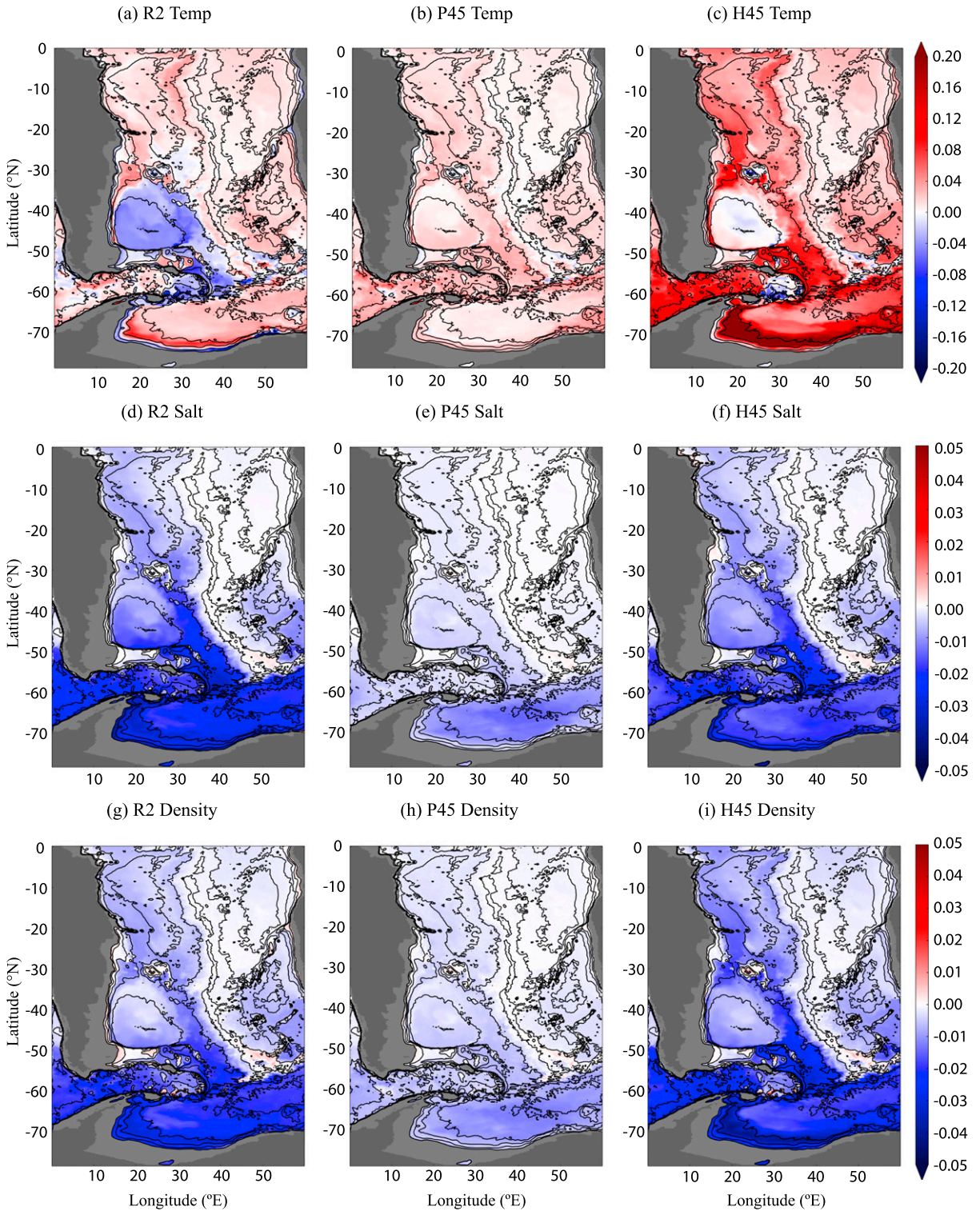

FIG. 9. Perturbation minus CTR in bottom-cell (a)–(c) temperature (°C), (d)–(f) salinity, and (g)–(i) potential density referenced to 2000 m (σ_2; kg m^{-3}) averaged over the last decade of the perturbation experiments for (left)–(right) cases R2, P45, and H45, respectively. Contours show depths from 1000 to 5000 m at 1000-m intervals.

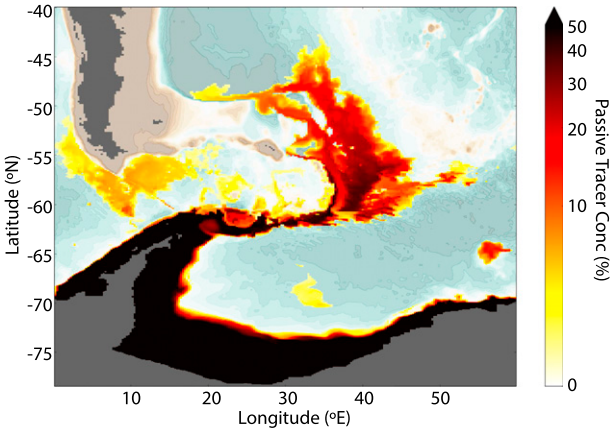

FIG. 10. Bottom gridcell concentration (%) of a passive tracer sourced on the Antarctic shelf, 10 years into the R2 perturbation run where the passive tracer was initialized during the start of the perturbation. Note that we have not shown the P45 and H45 cases because of strong similarities with the R2 case for the representation of bottom water pathways.

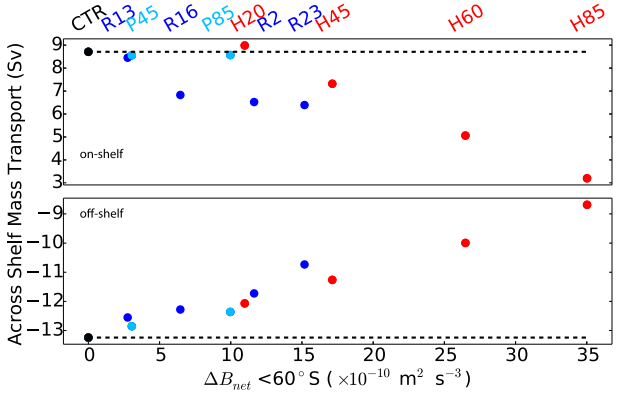

FIG. 11. Transport of waters across the Antarctic shelf edge (defined at 1000-m depth) below 500 m for each of the heat (red) and freshwater (blue) perturbation experiments averaged over the last 10 years of the experiments, with respect to change in net buoyancy flux of each perturbation. Positive transport indicates on-shelf flow and negative is off-shelf flow. On shelf indicates the sum of the mass transport directed up the topographic slope and off shelf the equivalent mass transport down slope. Dashed line shows the value of CTR. Details of the precipitation, runoff, and heat flux perturbations are given in Table 1.

Runoff, on the other hand, is sourced directly into the ocean shelf region and is not influenced by the sea ice condition. Such a distribution leads to a strong shelf cooling response and minimal open ocean warming (Fig. 8), allowing runoff to cause abyssal cooling south of 30°S for the entire perturbation period (Figs. 9a and 12a). The differing responses of precipitation to that of runoff highlight the importance of including local glacial runoff in climate simulations. Many previous studies investigating the influence of increased freshwater fluxes to the Southern Ocean focus on the impact of changes in precipitation. Our results highlight a limitation of many climate models, including those of CMIP5, as they are unable to simulate freshwater flux changes from increased glacial melt (Lavergne et al. 2014; van den Berk and Drijfhout 2014).

Increased heat fluxes, through influencing the sea ice condition as well as the ocean state, maintain significant changes over both the shelf and open ocean (Figs. 6c,f,i and 7c,f,i). These changes lead to strong shelf cooling and open ocean warming (Fig. 8). Through driving adjustments on both the shelf and open ocean, the cooling of the abyssal ocean is reversed in the final periods of the warming scenarios (Fig. 12a), consistent with increased penetration of warm waters over time. The overflowing shelf waters entrain the warming deep ocean waters, offsetting shelf cooling. Hence, through the different responses of the shelf source AABW versus that of the open ocean processes, a decadal-scale variability of the abyssal ocean is revealed. Such changes highlight the

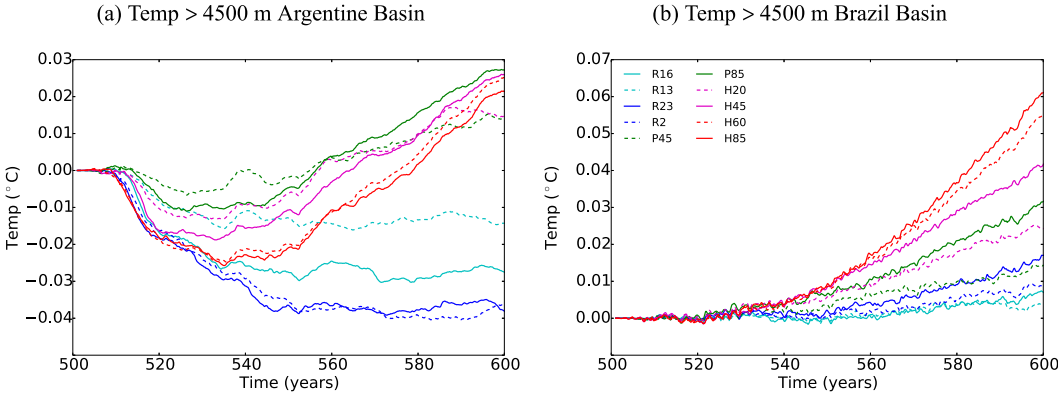

FIG. 12. Time series of changes in temperature (°C) from CTR for waters below 4500 m within (a) the Argentine basin and (b) the Brazil basin for each of the perturbation experiments.

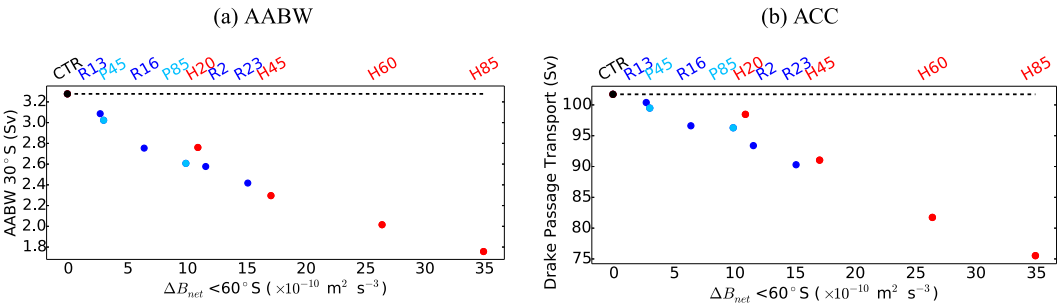

FIG. 13. (a) Magnitude of AABW transport at 30°S (defined as the minimum below 36.9 kg m^{-3} of the MOC in σ_2 space) and (b) total eastward Drake Passage transport for each of the heat (red) and freshwater (blue) perturbation experiments averaged over the last 10 years of the experiments, with respect to change in net buoyancy flux of each perturbation. Dashed line shows the value of CTR. Details of the precipitation, runoff, and heat flux perturbations are given in Table 1.

role of shelf water properties and exchange in driving AABW variability in conjunction with longer-term anthropogenic forcing.

Observations suggest a warming trend within the bottom water of the Argentine basin and Brazil basins (Coles et al. 1996; Johnson and Doney 2006; Johnson et al. 2014); however, there is evidence of cooling and freshening on AABW density surfaces having occurred during the 1980s in the Argentine region (Coles et al. 1996). Further, while a warming trend is evident from 1989 or 1995 to 2014 in the Argentine basin, no significant warming is observed from 2005 to 2014 (Johnson et al. 2014). The recent reduced warming of the Argentine basin has been proposed as a response to reduced inflow of AABW to the region (Johnson et al. 2014). Our results suggest an alternative mechanism to produce a period of reduced warming response in the Argentine basin, derived from the potential to cool shelf waters forming AABW (Fig. 12); that is, a change in onshore/offshore exchange can drive temporal variability in the Argentine basin.

Abyssal cooling in our simulations is confined to regions below 4000 m in the Argentine basin (R2; Fig. 7a). Hence, the warmer waters above may constitute a larger portion of AABW entering the Brazil basin as mixing occurs across the relatively shallow Vema Channel (depth of ~4600 m; Zenk and Morozov 2007). This mixing allows warming within the Vema Channel and Brazil basin (as found in observations; Zenk and Morozov 2007) for all simulations, despite the periods of cooling within the Argentine basin (Figs. 7 and 12a).

The cooling of dense shelf waters simulated in our model (Fig. 8, right) provides a mechanism explaining the observations of Azaneu et al. (2013). Inclusion of this mechanism requires shelf-sourced AABW to be correctly represented. Many climate models, and indeed those of the CMIP5 generation, rely primarily on open ocean convection for AABW formation (Heuzé et al. 2013, 2015). The different responses attainable by including shelf processes indicate a limitation of many climate models and emphasize the importance of incorporating shelf-sourced AABW in the bottom water formation process.

c. *Transport*

The strength of the AABW overturning cell in our model is controlled by both open ocean convection and dense water formation on the continental shelf. Observations indicate that 2–5 Sv of Weddell Sea bottom water (contributing to AABW) is drawn from the shelf and 1–3 Sv from the Weddell Gyre polynya in periods when open ocean convection is active (Gordon 2001). In our model, we calculate the fraction of open ocean to shelf-sourced AABW via comparison of vertical transports over which passive tracers sourced separately in the open ocean and shelf have mixed to depth. Specifically, we calculate the net volume flux flowing through 2000 m with tracer concentrations greater than 10%, averaged over years 501–503 of CTR (the passive tracer is sourced at the beginning of year 501). We use only the initial years because in subsequent years a significant amount of the shelf-sourced tracer has mixed into the open ocean and vice versa. This diagnostic indicates that open ocean convection in our model contributes to an upper limit of 20% of AABW formation, which is a similar fraction of shelf and open ocean convection to that observed.

Increased freshwater/heat fluxes to the ocean surface decrease AABW source water densities and hinder the onset of convection and descent of dense shelf waters. Both characteristics are derived from changes in the surface buoyancy fluxes and result in a decrease in AABW overturning. In fact, a near-linear reduction in AABW with increasing surface buoyancy south of 60°S is found for all perturbation cases (Fig. 13a). Decreased

AABW production has been observed in recent decades through a contraction of AABW density classes (Purkey and Johnson 2012). To understand the potential impact of reduced AABW transport on the climate, the causes of such changes must be quantified and correctly attributed. Our results show that surface buoyancy fluxes play a crucial role in controlling and influencing the lower overturning cell.

The strength of AABW overturning also influences the strength of the ACC (Gent et al. 2001). A reduced northward flow of AABW across the ACC decreases the Coriolis-induced westward-flowing waters. The westward-flowing abyssal layer is damped by form stresses and topographic drag. Such damping acts as an effective eastward momentum source, meaning reduced westward flow (via reduced northward AABW) acts as a relative sink of eastward momentum (Howard et al. 2015).

The influence of buoyancy in controlling the ACC strength is also well established (Aiken and England 2008; Hogg 2010). In our simulations, increased warming and freshening south of 60°S (Fig. 7) act to reduce the meridional pressure gradients across the ACC fronts. The flattening of pressure gradients decreases ACC flow as a result of geostrophy [similar results were found in Aiken and England (2008)]. Both reduced Southern Ocean density and AABW overturning contribute to a reduction in ACC transport such that greater surface buoyancy flux changes lead to larger reductions in ACC transport (Fig. 13b).

The role of winds in influencing ACC flow has not been considered in this study. Projected poleward shifts and increased wind stress over the Southern Ocean potentially increase the ACC strength (though the role of eddy saturation in hindering any such increase must also be taken into account; Meredith and Hogg 2006). Despite the potential influence of changing buoyancy, winds, and overturning on the ACC shown through numerous modeling studies, there is as yet no conclusive observational evidence supporting either an increase or a decrease in ACC transport through Drake Passage given the short observational time series currently available (e.g., Meredith et al. 2011; Hogg et al. 2015).

4. Discussion and conclusions

The sensitivity of AABW formation, properties, and deep stratification to surface buoyancy forcing in a realistic bathymetry, eddy-permitting sector ocean–ice model has been examined. Both surface heat and freshwater fluxes have been independently considered in evaluating changes to surface buoyancy. Upper-ocean temperature in the Southern Ocean decreases under increased freshwater fluxes, while enhanced precipitation increases total sea ice mass. Increased surface heat fluxes, on the other hand, facilitate upper-ocean warming while concurrently reducing total sea ice mass. Further, reduced total sea ice mass under heating induces a change in surface freshwater fluxes an order of magnitude larger than that produced via precipitation changes. The opposing responses of the different buoyancy flux components and the large buoyancy flux change induced under heating emphasizes the importance of including both heating and freshwater fluxes in capturing the complete, and complex, response of the drivers of AABW formation and properties.

Freshening of shelf and open ocean water masses (supporting recent observational evidence of AABW freshening; Aoki et al. 2005; Rintoul 2007; Purkey and Johnson 2010, 2013) through increased surface buoyancy fluxes decreases the volume of AABW source water and hinders the onset of convection (via strengthening of the halocline). Reduced shelf density and convection decreases AABW transport. The decreased AABW transport is found to be proportional to the net buoyancy flux changes (influenced through both freshwater and heat flux influences), emphasizing the underlying role buoyancy plays in defining bottom water properties and the meridional overturning circulation.

Inclusion of shelf-sourced AABW in our model (unlike in many climate models) facilitates a cooling of AABW source regions in response to atmospheric warming and increased glacial runoff. Cooling on the Antarctic shelves occurs as a result of decreased on-shelf/off-shelf exchange, reducing the volume of intruding warm Circumpolar Deep Water (CDW) onto the shelf. As the overflowing shelf waters descend the slope and entrain CDW, the cooler shelf waters oppose the deep ocean warming response, leading to periods of decreased temperatures in the deep Argentine basin. While runoff perturbations maintain abyssal cooling, continued deep ocean warming under increased heat fluxes eventually dominates over the dense shelf water cooling, leading to long-term net warming. The abyssal ocean response to the shelf cooling and open ocean warming presents a potential driver of decadal-scale variability of AABW properties.

The simulated dense shelf water cooling matches recent observational trends (Azaneu et al. 2013) while preserving the observed warming of the densest waters within the Vema Channel (Zenk and Morozov 2007). No previous work provides a mechanism that may explain the observed cooling of dense shelf waters around Antarctica along with continued far-field warming. Further, freshwater flux increases through precipitation are unable to attain equivalent responses on the shelf and deep ocean to that of increasing glacial runoff. Our

results show that including both shelf processes and glacial runoff in climate change simulations is essential to capture the complete spectrum of influences controlling AABW and abyssal stratification. Both factors are currently absent in most climate models and indeed those of the CMIP5 generation.

While the importance of shelf processes and the on-shelf/off-shelf exchange is maintained, we note that even at 0.25° resolution, eddy fluxes and their role in the exchange process are not fully resolved (Stewart and Thompson 2015). The key mechanism controlling shelf exchange within a realistic bathymetry and surface forcing model remains an important avenue for future work yet is beyond the scope of this study.

The lack of feedback and regional variability of the glacial runoff in our model presents a second limitation of our methods. A cooling on the shelf may in fact reduce the enhancement of basal melting, though consideration of ice-sheet stability must also be taken into account. The first steps to including regional varying freshwater fluxes from ice sheets in climate models is underway (van den Berk and Drijfhout 2014); however, further progress is needed to allow a fully coupled ice-sheet model within climate models.

Finally, since our study focused on buoyancy flux perturbations, the relative role of wind has not been assessed. We note that this limitation may influence the degree of change we find. For example, changes in the Southern Hemisphere westerly winds potentially play a role in Southern Ocean SST changes and on-shelf CDW flow (e.g., Lefebvre et al. 2004; Hogg et al. 2008; Thompson et al. 2011; Dinniman et al. 2012). However, the controlling role of buoyancy forces in inhibiting the shelf and deep ocean warming response alludes to the possibility that the deep ocean is experiencing a more accelerated state of warming than previously anticipated. Despite the absence of winds, we maintain that in order to suitably assess the ocean's state as a result of its response to anthropogenic influences on the climate, both shelf-sourced AABW and glacial runoff changes must be suitably incorporated into climate models.

Acknowledgments. We thank the three anonymous reviewers for their efforts and thoughtful comments. This work was undertaken using the National Facility of the National Computational Infrastructure at the ANU. BMS was supported by the Australian Government Department of the Environment and CSIRO through the Australian Climate Change Science Programme. AMH was supported by an Australian Research Council Future Fellowship FT120100842. SMD was supported by the Australian Government Business Cooperative Research Centres Programme through the Antarctic Climate and Ecosystems Cooperative Research Centre (ACE CRC).

REFERENCES

Aiken, C. M., and M. H. England, 2008: Sensitivity of the present-day climate to freshwater forcing associated with Antarctic sea ice loss. *J. Climate*, **21**, 3936–3946, doi:10.1175/2007JCLI1901.1.

Aoki, S., N. L. Bindoff, and J. A. Church, 2005: Interdecadal water mass changes in the Southern Ocean between 30°E and 160°E. *Geophys. Res. Lett.*, **32**, L07607, doi:10.1029/2004GL022220.

Azaneu, M., R. Kerr, M. M. Mata, and C. A. E. Garcia, 2013: Trends in the deep Southern Ocean (1958–2010): Implications for Antarctic Bottom Water properties and volume export. *Geophys. Res. Lett.*, **118**, 4213–4227, doi:10.1002/jgrc.20303.

Bintanja, R., G. J. van Oldenborgh, S. S. Drijfhout, B. Wouters, and C. A. Katsman, 2013: Important role for ocean warming and increased ice-shelf melt in Antarctic sea-ice expansion. *Nat. Geosci.*, **6**, 376–379, doi:10.1038/ngeo1767.

——, ——, and C. A. Katsman, 2015: The effect of increased fresh water from Antarctic ice shelves on future trends in Antarctic sea ice. *Ann. Glaciol.*, **56**, 120–126, doi:10.3189/2015AoG69A001.

Blunden, J., and Coauthors, 2014: State of the climate in 2013. *Bull. Amer. Meteor. Soc.*, **95** (7), S1–S257, doi:10.1175/2014BAMSStateoftheClimate.1.

Coles, V. J., M. S. McCartney, and D. B. Olson, 1996: Changes in Antarctic Bottom Water properties in the western South Atlantic in the late 1980s. *J. Geophys. Res.*, **101**, 8957–8970, doi:10.1029/95JC03721.

Delworth, T. L., and Coauthors, 2012: Simulated climate and climate change in the GFDL CM2.5 high-resolution coupled climate model. *J. Climate*, **25**, 2755–2781, doi:10.1175/JCLI-D-11-00316.1.

Dinniman, M. S., J. M. Klinck, and W. O. Smith Jr., 2011: A model study of Circumpolar Deep Water on the West Antarctic Peninsula and Ross Sea continental shelves. *Deep-Sea Res. II*, **58**, 1508–1523, doi:10.1016/j.dsr2.2010.11.013.

——, ——, and E. E. Hofmann, 2012: Sensitivity of Circumpolar Deep Water transport and ice shelf basal melt along the West Antarctic Peninsula to changes in the winds. *J. Climate*, **25**, 4799–4816, doi:10.1175/JCLI-D-11-00307.1.

England, M. H., 1993: Representing the global-scale water masses in ocean general circulation models. *J. Phys. Oceanogr.*, **23**, 1523–1552, doi:10.1175/1520-0485(1993)023<1523:RTGSWM>2.0.CO;2.

Fahrbach, E., M. Hoppema, G. Rohardt, M. Schröder, and A. Wisotzki, 2004: Decadal-scale variations of water mass properties in the deep Weddell Sea. *Ocean Dyn.*, **54**, 77–91, doi:10.1007/s10236-003-0082-3.

——, ——, ——, O. Boebel, O. Klatt, and A. Wisotzki, 2011: Warming of deep and abyssal water masses along the Greenwich meridian on decadal time scales: The Weddell gyre as a heat buffer. *Deep-Sea Res. II*, **58**, 2509–2523, doi:10.1016/j.dsr2.2011.06.007.

Fan, T., C. Deser, and D. P. Schneider, 2014: Recent Antarctic sea ice trends in the context of Southern Ocean surface climate variations since 1950. *Geophys. Res. Lett.*, **41**, 2419–2426, doi:10.1002/2014GL059239.

Ferreira, D., J. Marshall, C. M. Bitz, S. Solomon, and A. Plumb, 2015: Antarctic Ocean and sea ice response to ozone depletion:

A two-time-scale problem. *J. Climate*, **28**, 1206–1226, doi:10.1175/JCLI-D-14-00313.1.

Fox-Kemper, B., R. Ferrari, and R. W. Hallberg, 2008: Parameterization of mixed layer eddies. Part I: Theory and diagnosis. *J. Phys. Oceanogr.*, **38**, 1145–1165, doi:10.1175/2007JPO3792.1.

Gent, P., W. G. Large, and F. O. Bryan, 2001: What sets the mean transport through Drake Passage. *J. Geophys. Res.*, **106**, 2693–2712, doi:10.1029/2000JC900036.

Gordon, A. L., 2001: Bottom water formation. *Encyclopaedia of Ocean Sciences*, J. H. Steele, K. K. Turekian, and S. A. Thorpe, Eds., Academic Press, 334–340.

Griffies, S. M., 2012: Elements of the Modular Ocean Model (MOM). GFDL Ocean Group Tech. Rep. 7, NOAA/Geophysical Fluid Dynamics Laboratory, 618 pp. [Available online at http://www.mom-ocean.org/web/docs/project/MOM5_elements.pdf.]

Gwyther, D. E., B. K. Galton-Fenzi, J. R. Hunter, and J. L. Roberts, 2014: Simulated melt rates for the Totten and Dalton ice shelves. *Ocean Sci.*, **10**, 267–279, doi:10.5194/os-10-267-2014.

Hellmer, H. H., F. Kauker, R. Timmermann, J. Determann, and J. Rae, 2012: Twenty-first-century warming of a large Antarctic ice-shelf cavity by a redirected coastal current. *Nature*, **485**, 225–228, doi:10.1038/nature11064.

Heuzé, C., K. J. Heywood, D. P. Stevens, and J. K. Ridley, 2013: Southern Ocean bottom water characteristics in CMIP5 models. *Geophys. Res. Lett.*, **40**, 1409–1414, doi:10.1002/grl.50287.

——, ——, ——, and ——, 2015: Changes in global ocean bottom properties and volume transports in CMIP5 models under climate change scenarios. *J. Climate*, **28**, 2917–2944, doi:10.1175/JCLI-D-14-00381.1.

Hogg, A. M., 2010: An Antarctic Circumpolar Current driven by surface buoyancy forcing. *Geophys. Res. Lett.*, **37**, L23601, doi:10.1029/2010GL044777.

——, M. P. Meredith, J. R. Blundell, and C. Wilson, 2008: Eddy heat flux in the Southern Ocean: Response to variable wind forcing. *J. Climate*, **21**, 608–620, doi:10.1175/2007JCLI1925.1.

——, ——, D. P. Chambers, E. P. Abrahamsen, C. W. Hughes, and A. K. Morrison, 2015: Recent trends in the Southern Ocean eddy field. *J. Geophys. Res.*, **120**, 257–267, doi:10.1002/2014JC010470.

Howard, E., A. M. Hogg, S. Waterman, and D. Marshall, 2015: The injection of zonal momentum by buoyancy forcing in a Southern Ocean model. *J. Phys. Oceanogr.*, **45**, 259–271, doi:10.1175/JPO-D-14-0098.1.

IPCC, 2013: *Climate Change 2013: The Physical Science Basis*. Cambridge University Press, 1535 pp., doi:10.1017/CBO9781107415324.

Jacobs, S. S., 2004: Bottom water production and its links with the thermohaline circulation. *Antarct. Sci.*, **16**, 427–437, doi:10.1017/S095410200400224X.

——, A. Jenkins, C. F. Giulivi, and P. Dutrieux, 2011: Stronger ocean circulation and increased melting under Pine Island Glacier ice shelf. *Nat. Geosci.*, **4**, 519–523, doi:10.1038/ngeo1188.

Johnson, G. C., 2008: Quantifying Antarctic Bottom Water and North Atlantic Deep Water volumes. *J. Geophys. Res.*, **113**, C05027, doi:10.1029/2007JC004477.

——, and S. C. Doney, 2006: Recent western South Atlantic bottom water warming. *Geophys. Res. Lett.*, **33**, L14614, doi:10.1029/2006GL026769.

——, K. E. McTaggart, and R. Wanninkhof, 2014: Antarctic Bottom Water temperature changes in the western South Atlantic from 1989 to 2014. *J. Geophys. Res. Oceans*, **119**, 8567–8577, doi:10.1002/2014JC010367.

Joughin, I., R. B. Alley, and D. M. Holland, 2012: Ice-sheet response to oceanic forcing. *Science*, **338**, 1172–1176, doi:10.1126/science.1226481.

Jullion, L., A. C. N. Garabato, M. P. Meredith, P. R. Holland, P. Courtois, and B. A. King, 2013: Decadal freshening of the Antarctic Bottom Water exported from the Weddell Sea. *J. Climate*, **26**, 8111–8125, doi:10.1175/JCLI-D-12-00765.1.

Khazendar, A., M. P. Schodlok, I. Fenty, S. R. M. Ligtenberg, E. Rignot, and M. R. van den Broeke, 2013: Observed thinning of Totten Glacier is linked to coastal polynya variability. *Nat. Commun.*, **4**, 2857, doi:10.1038/ncomms3857.

Kirkman, C. H., and C. M. Bitz, 2011: The effect of the sea ice freshwater flux on Southern Ocean temperatures in CCSM3: Deep-ocean warming and delayed surface warming. *J. Climate*, **24**, 2224–2237, doi:10.1175/2010JCLI3625.1.

Kuhlbrodt, T., A. Griesel, M. Montoya, A. Levermann, M. Hofmann, and S. Rahmstorf, 2007: On the driving processes of the Atlantic meridional overturning circulation. *Rev. Geophys.*, **45**, RG2001, doi:10.1029/2004RG000166.

Large, W. G., and S. Yeager, 2009: The global climatology of an interannually varying air–sea flux data set. *Climate Dyn.*, **33**, 341–364, doi:10.1007/s00382-008-0441-3.

——, J. C. McWilliams, and S. C. Doney, 1994: Oceanic vertical mixing: A review and a model with a nonlocal boundary layer parameterization. *Rev. Geophys.*, **32**, 363–403, doi:10.1029/94RG01872.

Latif, M., T. Martin, and W. Park, 2013: Southern Ocean sector centennial climate variability and recent decadal trends. *J. Climate*, **26**, 7767–7782, doi:10.1175/JCLI-D-12-00281.1.

Lavergne, C., J. B. Palter, E. D. Galbraith, R. Bernardello, and I. Marinov, 2014: Cessation of deep convection in the open Southern Ocean under anthropogenic climate change. *Nat. Climate Sci.*, **4**, 278–282, doi:10.1038/nclimate2132.

Lee, H. C., A. Rosati, and M. J. Spelman, 2006: Barotropic tidal mixing effects in a coupled climate model: Oceanic conditions in the northern Atlantic. *Ocean Modell.*, **11**, 464–477, doi:10.1016/j.ocemod.2005.03.003.

Lefebvre, W., H. Goosse, and R. Timmermann, 2004: Influence of the southern annular mode on the sea ice-ocean system. *J. Geophys. Res.*, **109**, C09005, doi:10.1029/2004JC00240.

Ma, H., and L. Wu, 2011: Global teleconnections in response to freshening over the Antarctic Ocean. *J. Climate*, **24**, 1071–1088, doi:10.1175/2010JCLI3634.1.

Marshall, J., K. C. Armour, J. R. Scott, Y. Kostov, U. Hausmann, D. Ferreira, T. G. Shepherd, and C. M. Bitz, 2014: The ocean's role in polar climate change: Asymmetric Arctic and Antarctic responses to greenhouse gas and ozone forcing. *Philos. Trans. Roy. Soc. London*, **372A**, 20130040, doi:10.1098/rsta.2013.0040.

Martin, T., W. Park, and M. Latif, 2013: Multi-centennial variability controlled by Southern Ocean convection in the Kiel Climate Model. *Climate Dyn.*, **40**, 2005–2022, doi:10.1007/s00382-012-1586-7.

——, ——, and ——, 2015: Southern Ocean forcing of the North Atlantic at multi-centennial time scales in the Kiel Climate Model. *Deep-Sea Res. II*, **114**, 39–48, doi:10.1016/j.dsr2.2014.01.018.

Menviel, L., A. Timmermann, O. E. Timm, and A. Mouchet, 2010: Climate and biogeochemical response to a rapid melting of the West Antarctic ice sheet during interglacials and implications for future climate. *Paleoceanography*, **25**, PA4231, doi:10.1029/2009PA001892.

Meredith, M. P., and A. M. Hogg, 2006: Circumpolar response of Southern Ocean eddy activity to a change in the southern annular mode. *Geophys. Res. Lett.*, **33**, L16608, doi:10.1029/2006GL026499.

——, and Coauthors, 2011: Sustained monitoring of the Southern Ocean at Drake Passage: Past achievements and future priorities. *Rev. Geophys.*, **49**, RG4005, doi:10.1029/2010RG000348.

Morrison, A. K., A. M. Hogg, and M. L. Ward, 2011: Sensitivity of the Southern Ocean overturning circulation to surface buoyancy forcing. *Geophys. Res. Lett.*, **38**, L14602, doi:10.1029/2011GL048031.

——, M. H. England, and A. M. Hogg, 2015: Response of Southern Ocean convection and abyssal overturning to surface buoyancy perturbations. *J. Climate*, **28**, 4263–4278, doi:10.1175/JCLI-D-14-00110.1.

NOAA, 2001: 2-minute gridded global relief data (ETOPO2v2). National Geophysical Data Center. [Available online at http://www.ngdc.noaa.gov/mgg/fliers/01mgg04.html.]

Parkinson, C. L., and D. J. Cavalieri, 2012: Antarctic sea ice variability and trends, 1979–2010. *Cryosphere*, **6**, 871–880, doi:10.5194/tc-6-871-2012.

Pritchard, H. D., S. R. M. Ligtenberg, H. A. Fricker, D. V. Vaughan, M. R. van den Broeke, and L. Padman, 2012: Antarctic ice-sheet loss driven by basal melting of ice shelves. *Nature*, **484**, 502–505, doi:10.1038/nature10968.

Purkey, S. G., and G. C. Johnson, 2010: Warming of global abyssal and deep Southern Ocean waters between the 1990s and 2000s: Contributions to global heat and sea level rise budgets. *J. Climate*, **23**, 6336–6351, doi:10.1175/2010JCLI3682.1.

——, and ——, 2012: Global contraction of Antarctic Bottom Water between the 1980s and 2000s. *J. Climate*, **25**, 5830–5844, doi:10.1175/JCLI-D-11-00612.1.

——, and ——, 2013: Antarctic Bottom Water warming and freshening: Contributions to sea level rise, ocean freshwater budgets, and global heat gain. *J. Climate*, **26**, 6105–6122, doi:10.1175/JCLI-D-12-00834.1.

Rintoul, S. R., 2007: Rapid freshening of Antarctic Bottom Water formed in the Indian and Pacific Oceans. *Geophys. Res. Lett.*, **34**, L06606, doi:10.1029/2006GL028550.

Ríos, A. F., A. Velo, P. C. Pardo, M. Hoppema, and F. F. Pérez, 2012: An update of anthropogenic CO_2 storage rates in the western South Atlantic basin and the role of Antarctic Bottom Water. *J. Mar. Syst.*, **94**, 197–203, doi:10.1016/j.jmarsys.2011.11.023.

Robertson, R., M. Visbeck, A. L. Gordon, and E. Fahrbach, 2002: Long-term temperature trends in the deep waters of the Weddell Sea. *Deep-Sea Res. II*, **49**, 4791–4806, doi:10.1016/S0967-0645(02)00159-5.

Rye, C. D., A. C. N. Garabato, P. R. Holland, M. P. Meredith, A. J. G. Nurser, C. W. Hughes, A. C. Coward, and D. J. Webb, 2014: Rapid sea-level rise along the Antarctic margins in response to increased glacial discharge. *Nat. Geosci.*, **7**, 732–735, doi:10.1038/ngeo2230.

Seidov, D., E. Barron, and B. J. Haupt, 2001: Meltwater and the global ocean conveyor: Northern versus southern connections. *Global Planet. Change*, **30**, 257–270, doi:10.1016/S0921-8181(00)00087-4.

Simmons, H. L., S. R. Jayne, L. C. St. Laurent, and A. J. Weaver, 2004: Tidally driven mixing in a numerical model of the ocean general circulation. *Ocean Modell.*, **6**, 245–263, doi:10.1016/S1463-5003(03)00011-8.

Snow, K., A. M. Hogg, S. M. Downes, B. M. Sloyan, M. L. Bates, and S. M. Griffies, 2015: Sensitivity of abyssal water masses to overflow parameterisations. *Ocean Modell.*, **89**, 84–103, doi:10.1016/j.ocemod.2015.03.004.

Spence, P., O. A. Saenko, M. Eby, and A. J. Weaver, 2009: The Southern Ocean overturning: Parameterized versus permitted eddies. *J. Phys. Oceanogr.*, **39**, 1634–1651, doi:10.1175/2009JPO4120.1.

Stephens, G. L., M. Wild, P. W. Stackhouse Jr., T. L'Ecuyer, S. Kato, and D. S. Henderson, 2012: The global character of the flux of downward longwave radiation. *J. Climate*, **25**, 2329–2340, doi:10.1175/JCLI-D-11-00262.1.

Stewart, A. L., and A. F. Thompson, 2015: Eddy-mediated transport of warm Circumpolar Deep Water across the Antarctic Shelf Break. *Geophys. Res. Lett.*, **42**, 432–440, doi:10.1002/2014GL062281.

Swingedouw, D., T. Fichefet, H. Goosse, and M. F. Loutre, 2009: Impact of transient freshwater releases in the Southern Ocean on the AMOC and climate. *Climate Dyn.*, **33**, 365–381, doi:10.1007/s00382-008-0496-1.

Taylor, K. E., R. J. Stouffer, and G. A. Meehl, 2012: An overview of CMIP5 and the experiment design. *Bull. Amer. Meteor. Soc.*, **93**, 485–498, doi:10.1175/BAMS-D-11-00094.1.

Taylor, P. C., M. Cai, A. Hu, G. A. Meehl, W. Washington, and G. J. Zhang, 2013: A decomposition of feedback contributions to polar warming amplification. *J. Climate*, **26**, 7023–7043, doi:10.1175/JCLI-D-12-00696.1.

Thoma, M., A. Jenkins, D. Holland, and S. Jacobs, 2008: Modelling Circumpolar Deep Water intrusions on the Amundsen Sea continental shelf, Antarctica. *Geophys. Res. Lett.*, **35**, L18602, doi:10.1029/2008GL034939.

Thompson, D. W. J., S. Solomon, P. J. Kushner, M. H. England, K. M. Grise, and D. J. Karoly, 2011: Signatures of the Antarctic ozone hole in Southern Hemisphere surface climate change. *Nat. Geosci.*, **4**, 741–749, doi:10.1038/ngeo1296.

Trevena, J., W. P. Sijp, and M. H. England, 2008: Stability of Antarctic bottom water formation to freshwater fluxes and implications for global climate. *J. Climate*, **21**, 3310–3326, doi:10.1175/2007JCLI2212.1.

Turner, J., J. S. Hosking, T. Phillips, and G. J. Marshall, 2013: Temporal and spatial evolution of the Antarctic sea ice prior to the September 2012 record maximum extent. *Geophys. Res. Lett.*, **40**, 5894–5898, doi:10.1002/2013GL058371.

van den Berk, J., and S. S. Drijfhout, 2014: A realistic freshwater forcing protocol for ocean-coupled climate models. *Ocean Modell.*, **81**, 36–48, doi:10.1016/j.ocemod.2014.07.003.

Winton, M., 2000: A reformulated three-layer sea ice model. *J. Atmos. Oceanic Technol.*, **17**, 525–531, doi:10.1175/1520-0426(2000)017<0525:ARTLSI>2.0.CO;2.

Zelinka, M. D., and D. L. Hartmann, 2012: Climate feedbacks and their implications for poleward energy flux changes in a warming climate. *J. Climate*, **25**, 608–624, doi:10.1175/JCLI-D-11-00096.1.

Zenk, W., and E. Morozov, 2007: Decadal warming of the coldest Antarctic Bottom Water flow through the Vema Channel. *Geophys. Res. Lett.*, **34**, L14607, doi:10.1029/2007GL030340.

Zhang, J., 2007: Increasing Antarctic sea ice under warming atmospheric and oceanic conditions. *J. Climate*, **20**, 2515–2529, doi:10.1175/JCLI4136.1.

Zhang, Y., and G. K. Vallis, 2013: Ocean heat uptake in eddying and non-eddying ocean circulation models in a warming climate. *J. Phys. Oceanogr.*, **43**, 2211–2229, doi:10.1175/JPO-D-12-078.1.

Zunz, V., H. Goosse, and F. Massonet, 2013: How does internal variability influence the ability of CMIP5 models to reproduce the recent trend in Southern Ocean sea ice extent? *Cryosphere*, **7**, 451–468, doi:10.5194/tc-7-451-2013.